LETTER

Reducing the contact time of a bouncing drop

James C. Bird[1]*, Rajeev Dhiman[2]*†, Hyuk-Min Kwon[2]* & Kripa K. Varanasi[2]

Surfaces designed so that drops do not adhere to them but instead bounce off have received substantial attention because of their ability to stay dry[1–4], self-clean[5–7] and resist icing[8–10]. A drop striking a non-wetting surface of this type will spread out to a maximum diameter[11–14] and then recoil to such an extent that it completely rebounds and leaves the solid material[15–18]. The amount of time that the drop is in contact with the solid—the 'contact time'—depends on the inertia and capillarity of the drop[1], internal dissipation[19] and surface–liquid interactions[20–22]. And because contact time controls the extent to which mass, momentum and energy are exchanged between drop and surface[23], it is often advantageous to minimize it. The conventional approach has been to minimize surface–liquid interactions that can lead to contact line pinning[20–22]; but even in the absence of any surface interactions, drop hydrodynamics imposes a minimum contact time that was conventionally assumed to be attained with axisymmetrically spreading and recoiling drops[21,24]. Here we demonstrate that it is possible to reduce the contact time below this theoretical limit by using superhydrophobic surfaces with a morphology that redistributes the liquid mass and thereby alters the drop hydrodynamics. We show theoretically and experimentally that this approach allows us to reduce the overall contact time between a bouncing drop and a surface below what was previously thought possible.

Our experiments involve releasing a water drop (radius $R = 1.33$ mm, velocity $U = 1.2$ m s^{-1}) onto a superhydrophobic surface and filming the bounce dynamics with high-speed cameras (Fig. 1). The surface used is a laser-ablated silicon wafer coated with fluorosilane, with chemical hydrophobicity and microscopic texture ensuring its superhydrophobic character (Fig. 1a inset). On this surface, the impacting drop viewed from the side (Fig. 1a) spreads to a nearly uniform film, retracts, and then lifts off within 12.4 ms. Simultaneously acquired top-view images show nearly axisymmetric dynamics throughout the process (Fig. 1b), consistent with past experiments[15–18]. When the film is axisymmetric and uniformly thick, the edge retracts inward at a constant velocity and the centre remains stationary[25,26] (Fig. 1c). This retraction velocity decreases with certain texture–liquid interactions (such as pinning), increasing the contact time[20–22]. Theoretical models suggest that the shortest contact time is on a surface with the sparsest texture necessary to trap a thin layer of air[21,22]. As this limit is approached, the drop dynamics become increasingly axisymmetric. Therefore, it is tacitly assumed that the minimum contact time should occur for a drop that recoils axisymmetrically with a centre that remains stationary until engulfed by the retracting rim.

We explored as an alternative non-axisymmetric recoil, or centre-assisted recoil. The basic idea is that if the hydrodynamics are altered such that the drop retracts with the liquid near the centre assisting with the recoil (Fig. 1d), contact time might be reduced further. To activate the drop centre, we propose adding designed macrotextures to the non-wetting surface to trigger a controlled asymmetry and non-uniform velocity field (Fig. 1d) in the retracting film. The combination of faster velocities in thinner film sections and smaller distances along certain directions should reduce contact time below the axisymmetric case.
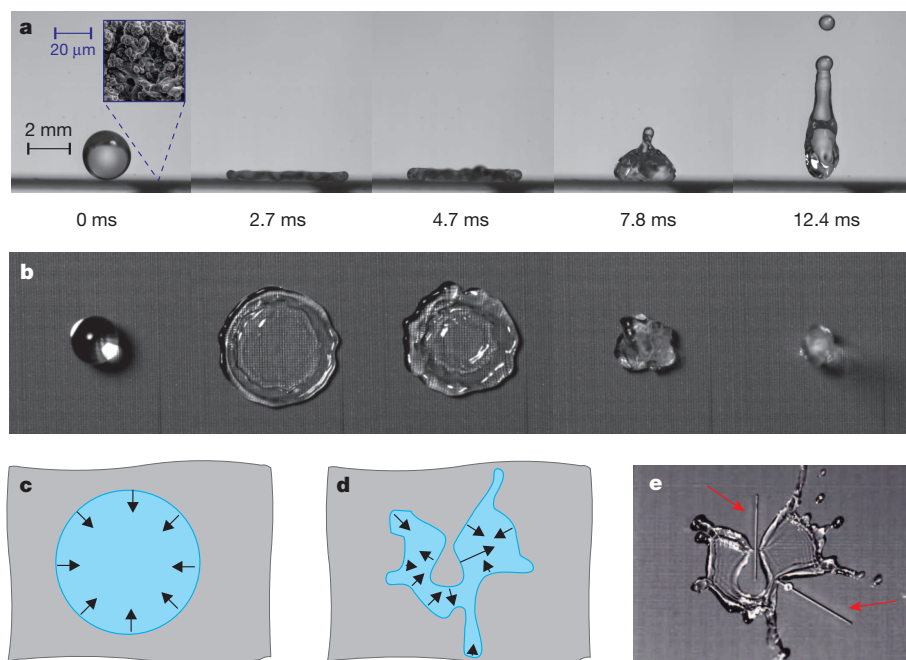

Figure 1 | A water drop bouncing on a superhydrophobic silicon surface. a, High-speed images of the bouncing show that the drop detaches from the surface after 12.4 ms (drop radius $R = 1.33$ mm; impact velocity $U = 1.2$ m s^{-1}). Inset, electron microscopy reveals the microscopic structure of the surface. **b,** Simultaneous top-view images demonstrate that the drop is nearly axisymmetric throughout the impact. **c,** The diagram portrays typical axisymmetric recoil with uniform retraction along the rim. **d,** A diagram portraying an arbitrary non-axisymmetric retraction in which the centre of the film assists in the recoil. **e,** Experimental evidence that such a recoil is possible when macrotexture (indicated by red arrows) is incorporated into the surface. For more details, see Supplementary Video 1.

[1]Department of Mechanical Engineering, Boston University, Boston, Massachusetts 02155, USA. [2]Department of Mechanical Engineering, Massachusetts Institute of Technology, Cambridge, Massachusetts 02139, USA. †Present address: 3M Purifications, Inc., 400 Research Parkway, Meriden, Connecticut 06033, USA.
*These authors contributed equally to this work.

The experimental demonstration of this concept uses an embossed macrotexture (indicated by red arrows in Fig. 1e) with an amplitude comparable to, but less than, the film thickness.

We promote non-axisymmetric centre-assisted recoil by spatially varying the film thickness, which can cause the retraction velocity to vary spatially. If the thickness h of the flattened drop were uniform, the rim should retract axisymmetrically with speed[25,26] $V = \sqrt{2\gamma/\rho h}$ (Fig. 2a, left), where γ is the liquid–air surface tension and ρ is the liquid density. However, if the thickness were not uniform, the retraction velocity would be faster in the thinner regions with less mass to accelerate (Fig. 2a, right). As the faster retracting fronts move along the peak of the macrotexture (ridge), the centre opens, fragmenting the drop and decreasing the distance and time required for recoil.

We accordingly fabricated a superhydrophobic surface with two distinct length scales (Fig. 2b). The smaller length scale consists of hierarchical micrometre-scale and nanometre-scale features identical to those used in Fig 1a, b, imparting superhydrophobicity with minimal pinning.
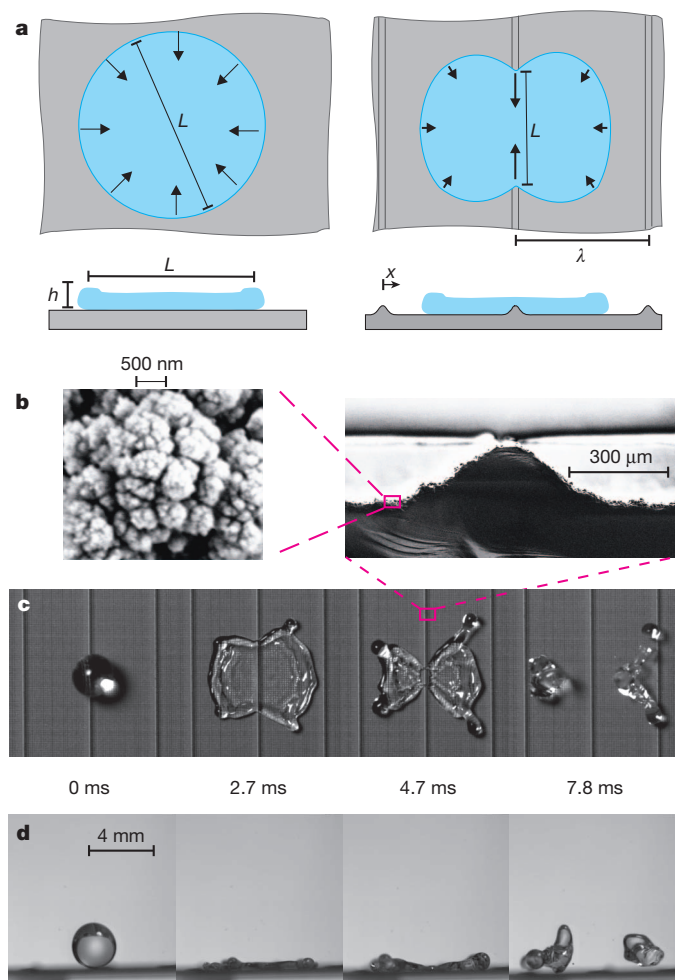
Figure 2 | Non-axisymmetric recoil can shorten contact time. a, The retraction speed of a film increases with decreasing thickness. Left and right, diagrams of a macroscopically untextured surface and a macroscale textured surface, respectively; top and bottom, top-view and side-view diagrams illustrating how macroscale texturing can modify the thickness profile of the drop, leading to variations in recoil speed (indicated by the length of the arrows). **b,** As shown in these SEM images, we have fabricated a silicon surface with both submicrometre roughness and structure on a macroscopic ($\sim$100 µm) scale by laser ablation. **c,** When a drop impacts the surface with the macroscopic structure, it moves rapidly along the ridge as it recoils. **d,** Simultaneous high-speed images captured from the side reveal that the overall contact time is reduced by 37% to 7.8 ms. For more details, see Supplementary Videos 2, 3.

The larger length scale consists of macroscopic features approaching the length scale of the film thickness h (Fig. 2b) for modifying the retraction hydrodynamics. The macrotexture height z varies as $z = a \sin^n(x/\lambda)$, where x is the horizontal distance, $a = 150$ µm, $n = 100$ and $\lambda = 4$ mm (see Methods).

Top-view images of a drop recoiling on the macrotexture show faster retraction along the ridge than in other directions (Fig. 2c). This variation in speed breaks the radial symmetry of the recoiling film, causing the liquid to move rapidly inward along the ridge such that more of the film participates in the recoil. Note that the drop is not split before impact, but divides during recoil as a result of the modified hydrodynamics. Synchronized side-view images of this drop (Fig. 2d) verify that the overall contact time is less than that on the same surface without the macrotextures (Fig. 1b).

Previous experiments indicate that the drop contact time t_c is independent of the dimensionless Weber number, We ($\equiv \rho U^2 R/\gamma$); instead, it scales with the inertial-capillary timescale[1,21], $\tau \equiv \sqrt{\rho R^3/\gamma}$. To enable comparisons, we therefore report our contact times relative to τ. The minimum contact time for low-deformation impact (We < 1) can be approximated by the lowest-order oscillation period for a spherical drop[27], $t_c/\tau = \pi/\sqrt{2} \approx 2.2$. For large-deformation impact (We > 1), the contact time is similar even though the dynamics are distinctly different[1]. Indeed, to the best of our knowledge, every past experiment documenting a drop bouncing on passive surface—including Leidenfrost drops[28]—has reported a contact time greater than $t_c/\tau = 2.2$ (Extended Data Table 1), which translates to between 12 and 13 ms in our experiments.

A typical way to convey drop impact dynamics is to plot the radius of the wetted area as a function of time (Fig. 3a). Because of symmetry about the ridge, we find it most instructive to track the motion of the film perpendicular to the ridge, using the same axis when tracking the drop on the control surface. Inspection of the dynamics on the control surface (filled red squares in Fig. 3a) indicates that the drop first spreads to 2.5 times its initial radius and then recoils at a nearly constant rate, slowing down slightly when the flattened drop can no longer be approximated by a thin film ($r/R \approx 1$). At dimensionless time $t/\tau = 2.2$, the wetting radii in opposing directions contact, and the drop leaves the control surface.

The dynamics for the macrotextured surface are slightly more complex. The drop initially spreads over a time $T_s = 0.63$ and then begins to recoil (black filled circles in Fig. 3a). During the next time interval T_1, the film recoils along the ridge faster than it recoils perpendicular to the ridge, splitting into two drop fragments (Fig. 2c). At this point, the outer rim of the initial drop continues to recoil inward while the newly formed inward rim recoils outward. This combined inward and outward recoil continues over the time interval T_2. At dimensionless time $t/\tau = 1.3$, one of the fragments lifts off the surface and at $t/\tau = 1.4$, the remaining fragment lifts off. We denote the difference in contact time on the two surfaces as ΔT.

One might be tempted to rationalize this reduction, ΔT, by modifying the radius in the theoretical scaling to reduce the drop volume by half. However, this approach is not physically appropriate because the drop splits after it has spread out (Fig. 2c). Therefore, the film thickness depends on the initial radius, as opposed to the reduced radius (Supplementary Information, Extended Data Fig. 7). A better approach is to estimate ΔT using a hydrodynamic model that combines thin-film retraction, conservation of mass, and variations in film thickness due to the macrotexture. First, we note that the axisymmetric dimensionless retraction time on the control surface can be expressed as $T_r = T_1 + T_2 + \Delta T = r_{max}/V\tau$, where r_{max} is the maximum wetting radius and V is the average retraction velocity. Next, we approximate the ridge dewetting time as $T_1 \approx r_{max}/(V_p\tau)$, where V_p is the retraction velocity along the peak of the macrotexture. Finally, we estimate the interval over which the fragmented drops retract as $T_2 \approx (r_{max} - VT_1\tau)/(2V\tau)$. Here we have assumed the velocity of the outward rim and the newly-formed inward rim to be equal to each other and to the velocity of the axisymmetric control film. This
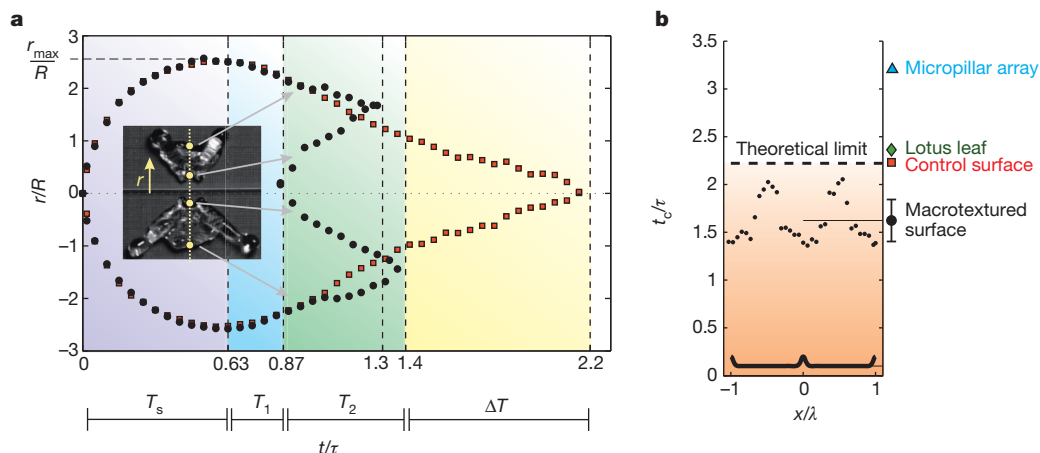
Figure 3 | The effect of macrotexture on drop impact dynamics and contact time. a, Plot of the contact line position (r; see inset) of a water drop impacting the control surface in Fig. 1 (red squares) and the macrotextured surface in Fig. 2 (black circles). The shaded regions highlight the various timescales (T_s, T_1, T_2, ΔT) relevant to our model. See text for details. **b**, Unlike the solely micro-nanotextured surfaces, the contact time of a drop on the macrotextured surface (indicated by black dots) depends on where it lands along the periodic macrotexture (indicated by the thick line at the bottom). The average

contact time over the entire surface is shorter than that of non-macrotextured surfaces (error bars denote one standard deviation). The filled symbols depict the contact time on various superhydrophobic surfaces, including a micropillar array, a lotus leaf, and a control surface. 'Theoretical limit' refers to $t_c/\tau = 2.2$ as discussed in the text. The elapsed time t and contact time t_c are made non-dimensional by dividing by $\tau = \sqrt{\rho R^3/\gamma}$, the radius r is normalized by the drop radius R, and the distance along the surface x is normalized by the macrotexture wavelength λ.

approximation is reasonable, given our expectation of nearly uniform film thickness ($\sim h$), with the exception of the top of the ridge. Thus the thin-film retraction speed away from the ridge is approximately $V \approx \sqrt{2\gamma/(\rho h)}$, and the speed on the macrotexture peak is $V_p \approx \sqrt{(2\gamma)/[\rho(h-a)]}$, where a is the macrotexture amplitude. After noting that mass conservation requires $(4/3)\pi R^3 \rho \approx \pi r_{max}^2 h\rho$, the previous expressions combine to reveal that $\Delta T \approx \frac{\sqrt{6}}{6}\left(1 - \sqrt{1 - \frac{a}{h}}\right)$. If there is no macrotexture ($a = 0$), then there is no contact time reduction ($\Delta T = 0$). If the macrotexture amplitude is equal to or greater than the film thickness ($a = h$), then the hydrodynamic model predicts a contact time reduction of $\Delta t_c \approx 0.4\tau$.

As Fig. 3 reveals, the model provides the correct order of magnitude, but underestimates the actual reduction by a factor of ~ 2. This difference is due to assumptions that are visible in Fig. 3a. First, the retraction velocity is slower than predicted[25,26] when the thin-film assumption breaks down. Second, the velocities of the inner and outer fronts are different, because the film thickness is not uniform. Last, the film away from the ridge spreads out further than the film on the ridge (Fig. 2c), resulting in an over-prediction of T_1 and under-prediction of ΔT. Nevertheless, the model elucidates the mechanism that reduces the overall contact time.

Careful inspection of Fig. 3a reveals that the two fragments leave the surface at slightly different times because the drop impacts the ridge slightly off-centre. At larger deviations from the ridge, this difference between the fragment lift-off times is more pronounced, increasing the overall contact time. The dimensionless contact times t_c/τ are reported for various landing locations along the periodic macrotexture x/λ (Fig. 3b). The contact time is shortest when the drop impacts directly on the ridge, increasing as the drop lands further away from the ridge, and then decreasing as the drop approaches the next ridge. By averaging over the wavelength, we find that the mean contact time over the entire surface is $t_c/\tau = 1.6$ with standard deviation $\sigma = 0.2$, a time significantly shorter than that on the control surface (Fig. 3b). For comparison, a drop under identical conditions contacted a lotus leaf for $t_c/\tau = 2.3$ and a micropillar array for $t_c/\tau = 3.2$ (Fig. 3b; Supplementary Video 3).

To confirm that the reduction in contact time is a result of the macrotexture geometry, and therefore a general phenomenon, we fabricated similar macrotextures in aluminium and copper by milling

ridges followed by microtexturing and coating with fluorosilane (Fig. 4a, b; Extended Data Figs 4, 5). The recoil dynamics are similar to those obtained on the macrotextured laser-ablated silicon surface (Fig. 2c; Fig. 4a, b).

We have searched to see if a similar system might exist in nature. We discovered that both the wings of the Morpho butterfly (*Morpho didius*) and the leaves of the nasturtium plant (*Tropaeolum majus L.*) have multiple superhydrophobic ridges, or veins, on a similar scale to our macrotextured surfaces. We find that centre-assisted recoil extends to
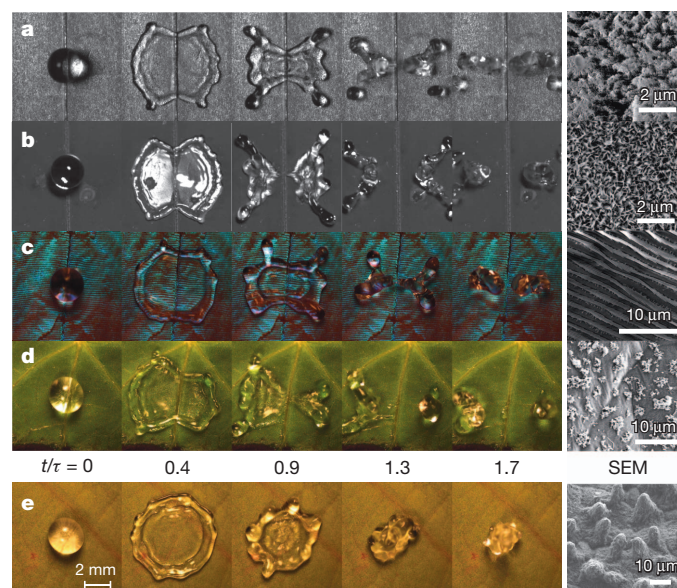

Figure 4 | Recoil dynamics generalize to a wide range of materials and microtextures. The figure shows top-view images of droplets impacting various surfaces; the SEM images of their respective microtextures are shown in the rightmost column. **a**, Anodized aluminium oxide with a milled macroscopic texture, pitted microtexture and a fluorinated coating. **b**, Etched copper oxide with a milled macroscopic texture, spiked microtexture and a fluorinated coating. **c**, A vein on the wing of a Morpho butterfly (*M. didius*). **d**, A vein on a nasturtium leaf (*T. majus L.*). **e**, For comparison, the same drop on a lotus leaf exhibits axisymmetric recoil. For all cases, We = 30. For more details, see Supplementary Video 4.

these surfaces as well (Fig. 4c, d; Extended Data Fig. 6), and that the overall drop contact time is significantly reduced from that of impact on macroscopically smooth surfaces, such as the lotus leaf, often considered the 'gold standard' of superhydrophobic surfaces (Fig. 4e). Further studies are needed to determine if there are any advantages for certain biological surfaces to contain these structures.

Although we have focused on a specific macrotexture that creates two distinct retraction velocities, centre-assisted recoil can occur for other macrotextures that modify the retraction hydrodynamics (such as Fig. 1e). These surfaces can be designed to reduce the drop contact time relative to other significant timescales, such as freezing. Indeed, molten tin drops impacting such surfaces are able to bounce off the surface before solidification (Supplementary Information, Extended Data Figs 1, 2, 3) and we expect that this approach could be extended to surfaces exposed to freezing rain to prevent icing. The new class of non-wetting surfaces that we present here could be useful for applications where staying dry under drop impingement is beneficial[8–10,29,30].

METHODS SUMMARY

The contact time of bouncing drops was obtained from the sequence of simultaneous top- and side-view images of drop impact captured by two high-speed cameras. The control and macrotextured ridge silicon surfaces were fabricated by ablating the surface using a Nd:YAG laser. The textured aluminium surface (Extended Data Fig. 4) was fabricated by milling ridges in aluminium and then performing a two-step anodization process consisting of polishing and etching. The textured copper oxide surface (Extended Data Fig. 5) was fabricated by milling ridges in copper and then treating with sodium hydroxide solution. All of the surfaces were coated with fluorosilane to render them superhydrophobic.

Online Content Any additional Methods, Extended Data display items and Source Data are available in the online version of the paper; references unique to these sections appear only in the online paper.

1. Richard, D., Clanet, C. & Quéré, D. Contact time of a bouncing drop. *Nature* **417**, 811 (2002).
2. de Gennes, P. G., Brochard-Wyart, F. & Quéré, D. *Capillarity and Wetting Phenomena* (Springer, 2004).
3. Gao, X. F. & Jiang, L. Water-repellent legs of water striders. *Nature* **432**, 36 (2004).
4. Quéré, D. Non-sticking drops. *Rep. Prog. Phys.* **68**, 2495–2532 (2005).
5. Blossey, R. Self-cleaning surfaces — virtual realities. *Nature Mater.* **2**, 301–306 (2003).
6. Tuteja, A. *et al.* Designing superoleophobic surfaces. *Science* **318**, 1618–1622 (2007).
7. Deng, X., Mammen, L., Butt, H. J. & Vollmer, D. Candle soot as a template for a transparent robust superamphiphobic coating. *Science* **335**, 67–70 (2012).
8. Mishchenko, L. *et al.* Design of ice-free nanostructured surfaces based on repulsion of impacting water droplets. *ACS Nano* **4**, 7699–7707 (2010).
9. Meuler, A. J., McKinley, G. H. & Cohen, R. E. Exploiting topographical texture to impart icephobicity. *ACS Nano* **4**, 7048–7052 (2010).
10. Jung, S., Tiwari, M. K., Doan, N. V. & Poulikakos, D. Mechanism of supercooled droplet freezing on surfaces. *Nature Commun.* **3**, 615 (2012).
11. Chandra, S. & Avedisian, C. T. On the collision of a droplet with a solid surface. *Proc. R. Soc. Lond. A* **432**, 13–41 (1991).
12. Clanet, C., Beguin, C., Richard, D. & Quéré, D. Maximal deformation of an impacting drop. *J. Fluid Mech.* **517**, 199–208 (2004).
13. Rein, M. Phenomena of liquid-drop impact on solid and liquid surfaces. *Fluid Dyn. Res.* **12**, 61–93 (1993).
14. Eggers, J., Fontelos, M. A., Josserand, C. & Zaleski, S. Drop dynamics after impact on a solid wall: theory and simulations. *Phys. Fluids* **22**, 062101 (2010).
15. Richard, D. & Quéré, D. Bouncing water drops. *Europhys. Lett.* **50**, 769–775 (2000).
16. Bartolo, D. *et al.* Bouncing or sticky droplets: impalement transitions on superhydrophobic micropatterned surfaces. *Europhys. Lett.* **74**, 299–305 (2006).
17. Deng, T. *et al.* Nonwetting of impinging droplets on textured surfaces. *Appl. Phys. Lett.* **94**, 133109 (2009).
18. Kwon, Y., Patankar, N., Choi, J. & Lee, J. Design of surface hierarchy for extreme hydrophobicity. *Langmuir* **25**, 6129–6136 (2009).
19. Bergeron, V., Bonn, D., Martin, J. Y. & Vovelle, L. Controlling droplet deposition with polymer additives. *Nature* **405**, 772–775 (2000).
20. Bartolo, D., Josserand, C. & Bonn, D. Retraction dynamics of aqueous drops upon impact on non-wetting surfaces. *J. Fluid Mech.* **545**, 329–338 (2005).
21. Reyssat, M., Richard, D., Clanet, C. & Quéré, D. Dynamical superhydrophobicity. *Faraday Discuss.* **146**, 19–33 (2010).
22. Li, X. Y., Ma, X. H. & Lan, Z. Dynamic behavior of the water droplet impact on a textured hydrophobic/superhydrophobic surface: the effect of the remaining liquid film arising on the pillars' tops on the contact time. *Langmuir* **26**, 4831–4838 (2010).
23. Bird, R. B., Stewart, W. E. & Lightfoot, E. N. *Transport Phenomena* (Wiley, 1960).
24. Okumura, K., Chevy, F., Richard, D., Quéré, D. & Clanet, C. Water spring: a model for bouncing drops. *Europhys. Lett.* **62**, 237–243 (2003).
25. Taylor, G. The dynamics of thin sheets of fluid. III. Disintegration of fluid sheets. *Proc. R. Soc. Lond. A* **253**, 313–321 (1959).
26. Culick, F. E. C. Comments on a ruptured soap film. *J. Appl. Phys.* **31**, 1128–1129 (1960).
27. Rayleigh, L. On the capillary phenomena of jets. *Proc. R. Soc. Lond.* **29**, 71–97 (1879).
28. Wachters, L. H. J. & Westerling, N. A. J. The heat transfer from a hot wall to impinging water drops in the spheroidal state. *Chem. Eng. Sci.* **21**, 1047–1056 (1966).
29. Corrigan, R. D. & DeMiglio, R. D. *Effect of Precipitation on Wind Turbine Performance*. Report No. NASA-TM-86986 (NASA, 1985).
30. Cotton, K. C. *Evaluating and Improving Steam Turbine Performance* (Cotton Fact, 1993).

Author Contributions J.C.B., R.D., H.-M.K. and K.K.V. designed the research; J.C.B., R.D. and H.-M.K. performed the research; J.C.B., R.D., H.-M.K. and K.K.V. analysed the data; J.C.B. wrote the original manuscript and all authors helped revise it. K.K.V. supervised the research.

Author Information Reprints and permissions information is available at www.nature.com/reprints. The authors declare no competing financial interests. Readers are welcome to comment on the online version of the paper. Correspondence and requests for materials should be addressed to K.K.V. (varanasi@mit.edu).

METHODS

Drop bouncing and imaging. Simultaneous top and side views of drop impact were captured with two high-speed cameras, each filming at a minimum of 10,000 frames per second. A combination of high-speed cameras (Photron S1, Phantom v7 and Colour Phantom v5) were used in these experiments. The drops were released from a needle at a fixed height above the surface. The size of the drop, the impact velocity and the contact time were calculated directly from the high-speed images for each trial.

Laser-ablated silicon surfaces. Control surfaces were fabricated by irradiating silicon surfaces with 100-ns pulses at a repetition rate of 20 kHz from an Nd:YAG laser at 1,064 nm wavelength and 150 W maximum continuous output. The surface was kept normal to the direction of the incident beam. Desired patterns were produced by rastering the laser beam with multiple steps. After coating with trichloro(1H,1H,2H,2H-perfluorooctyl)silane, the surface became superhydrophobic with an advancing contact angle of $\sim163°$ and a receding contact angle of $\sim161°$. These surfaces (control) display minimal pinning, as indicated by the extremely low contact angle hysteresis, $\sim2°$.

The ridge surface was designed such that the height varies as $z = a\,\sin^n(x/\lambda)$, where x is the horizontal distance and a, n and λ are constant parameters. The values of these parameters were selected as $\lambda = 4$ mm (to allow the drop to interact with one or two peaks regardless of impact locations), $a = 150\,\mu m$ (to provide a feature amplitude large enough to influence the film thickness h) and $n = 100$ (to restrict the full-width at half-maximum of the texture to 300 μm, a value small enough not to significantly influence the film thickness h away from the peak).

Silicon micropillar surface. The silicon micropillar array used in the experiments was fabricated using standard photolithography processes. A photomask with square windows was used and the pattern was transferred to photoresist using ultraviolet light exposure. Next, reactive ion etching in inductively coupled plasma was used to etch the exposed areas to form micropillars (each micropillar was 10 μm square with 10 μm height and was separated from the next pillar by 5 μm). Trichloro(1H,1H,2H,2H-perfluorooctyl)silane was coated onto the micropillars using vapour-phase deposition to render the surface superhydrophobic (advancing contact angle $\sim165°$, receding contact angle $\sim132°$).

Anodized aluminium oxide surface. The anodized aluminium oxide (AAO) surface was prepared by a two-step anodization and etching process. A 40 mm × 40 mm square and 5 mm thick piece of aluminium (grade 6061) was milled in a CNC machine to have ridges of 100 μm height and 200 μm width, as shown in Extended Data Fig. 4a. The surface was then thoroughly cleaned by first sonicating in acetone followed by rinsing with ethanol and distilled water and drying with nitrogen. The surface was first electropolished with a mixture of perchloric acid and ethanol (in a ratio of 1:3, respectively) for 20 min at 20 V and 100 mA. During this process, the mixture was stirred and maintained at 7 °C with the help of a stirrer plate. The surface was then washed several times with distilled water and then dried using nitrogen. After electropolishing, the surface was anodized with phosphoric acid for one hour at 40 V while the acid was continuously stirred and maintained at 15 °C. The surface was again thoroughly washed with distilled water and dried with nitrogen. The surface was then ready for etching, which was done with a mixture of chromic and phosphoric acids that were dissolved in distilled water in a proportion of 1.6 wt% and 6 wt%, respectively. The etching was done for 45 min while the mixture was maintained at 65 °C and continuously stirred. After this step, the surface was thoroughly washed with distilled water, dried with nitrogen and kept overnight in a refrigerator. The etching step was repeated at the same conditions for 2 h. Finally, the surface was cleaned thoroughly with distilled water and dried with nitrogen. SEM images (Extended Data Fig. 4b, c) of the anodized surface reveal that it has a hierarchical structure consisting of micropits (~ 10–$50\,\mu m$) and nanometre-scale pores (~50–100 nm). A drop of water placed on the surface spread completely, indicating that the surface was superhydrophilic. To render the surface hydrophobic, it was coated with trichloro(1H,1H,2H,2H-perfluorooctyl)silane using vapour-phase deposition. To characterize the hydrophobicity, contact angles were measured with a goniometer and found to be about 159° (advancing) and 157° (receding), indicating the surface was superhydrophobic with minimal pinning.

Copper oxide surface. The 100 μm high and 200 μm wide ridges were milled on a copper block, as for the AAO surface. Then, the following steps[31] were carried out to fabricate spiky nanostructures on the surface. The milled copper plate was ultrasonically cleaned in 3 M hydrochloric acid for 10 min, and rinsed with deionized water. Then, the plate was treated in a 30 mM sodium hydroxide solution, kept at 60 °C, for 20 h, followed by multiple rinses with deionized water and drying with nitrogen. The treated surface shows spike-like nano-scale textures, shown in Extended Data Fig. 5. Then, the surface was coated with trichloro(1H,1H,2H,2H-perfluorooctyl)silane using vapour-phase deposition to render it superhydrophobic.

31. Liu, J. *et al.* Hierarchical nanostructures of cupric oxide on a copper substrate: controllable morphology and wettability. *J. Mater. Chem.* **16,** 4427–4434 (2006).
32. Aziz, S. D. & Chandra, S. Impact, recoil, and splashing of molten metal droplets. *Int. J. Heat Mass Transfer* **43,** 2841–2857 (2000).
33. Legendre, D., Daniel, C. & Guiraud, P. Experimental study of a drop bouncing on a wall in a liquid. *Phys. Fluids* **17,** 097105 (2005).
34. Reyssat, M., Pépin, A., Marty, F., Chen, Y. & Quéré, D. Bouncing transitions on microtextured materials. *Europhys. Lett.* **74,** 306 (2006).
35. Jung, Y. C. & Bhushan, B. Dynamic effects of bouncing water droplets on superhydrophobic surfaces. *Langmuir* **24,** 6262–6269 (2008).
36. Brunet, P., Lapierre, F., Thomy, V., Coffinier, Y. & Boukherroub, R. Extreme resistance of superhydrophobic surfaces to impalement: reversible electrowetting related to the impacting/bouncing drop test. *Langmuir* **24,** 11203–11208 (2008).
37. Tuteja, A., Choi, W., Mabry, J., McKinley, G. H. & Cohen, R. E. Robust omniphobic surfaces. *Proc. Natl Acad. Sci. USA* **105,** 18200–18205 (2008).
38. Tsai, P., Pacheco, S., Pirat, C., Lefferts, L. & Lohse, D. Drop impact upon micro- and nanostructured superhydrophobic surfaces. *Langmuir* **25,** 12293–12298 (2009).
39. Zou, J., Wang, P. F., Zhang, T. R., Fu, X. & Ruan, X. Experimental study of a drop bouncing on a liquid surface. *Phys. Fluids* **23,** 044101 (2011).
40. Kwon, D. H. & Lee, S. J. Impact and wetting behaviors of impinging microdroplets on superhydrophobic textured surfaces. *Appl. Phys. Lett.* **100,** 171601 (2012).

3 mm

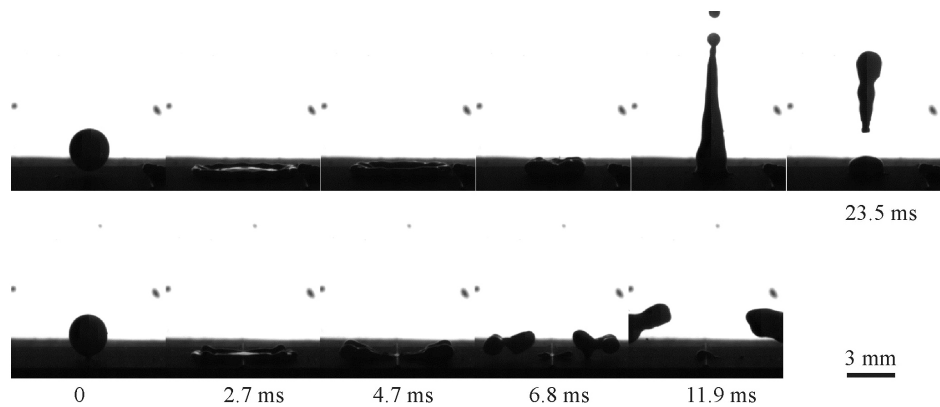| 0 | 2.7 ms | 4.7 ms | 6.8 ms | 11.9 ms |
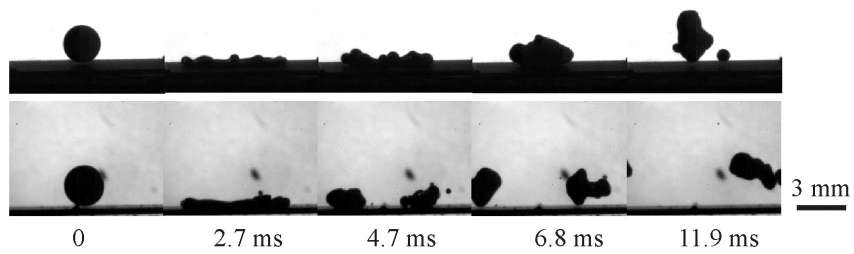
Extended Data Figure 1 | Impact of molten tin droplets (250 °C) on microscopically textured silicon substrates without (top row) and with (bottom row) macroscopic ridges. The substrate temperature is 150 °C, 82 °C below the droplet freezing point. In both cases, the droplets are able to bounce off the substrate.

29.2 ms

3 mm

0   2.7 ms   4.7 ms   6.8 ms   11.9 ms
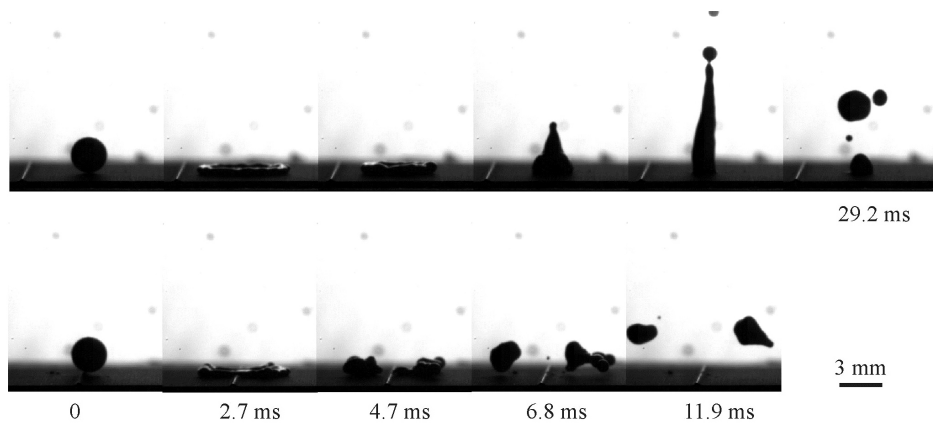
Extended Data Figure 2 | Impact of molten tin droplets (250 °C) on microscopically textured silicon substrates without contacting (top row) and contacting (bottom row) a macroscopic ridge. Here the substrate is maintained at 125 °C (a subcooling of 107 °C). When the droplet hits the macroscopic ridge, it is able to bounce off in 6.8 ms, whereas when impact is not on the ridge, the droplet is arrested owing to solidification. For more details, see Supplementary Video 5.

23.5 ms

3 mm

0   2.7 ms   4.7 ms   6.8 ms   11.9 ms

Extended Data Figure 3 | Impact of molten tin droplets (250 °C) on microscopically textured silicon substrates without (top row) and with (bottom row) ridges. Droplets impacting the ridge surface continued to bounce off until the substrate was cooled to about 50 °C, indicating that a significantly large subcooling (~182 °C) is needed to arrest the droplets on the ridge surface. Droplets impacting the surface without ridges (maintained at 50 °C) is arrested owing to solidification.
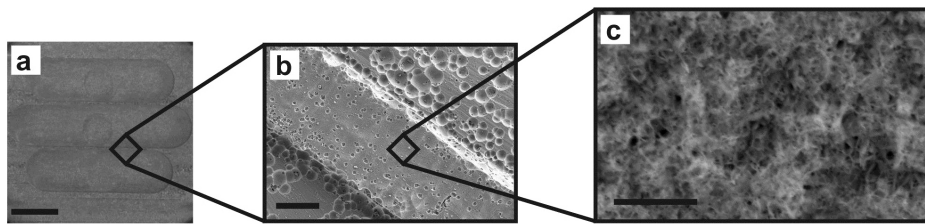
Extended Data Figure 4 | Images of AAO substrate surface at different magnifications. a, Top view of the anodized aluminium oxide (AAO) surface showing the macro-scale ridges (height ∼100 μm, width ∼200 μm); scale bar, 5 mm. **b**, Magnified SEM image of a single ridge showing micropits; scale bar, 100 μm. **c**, Further magnified SEM image showing nanoscale pores; scale bar, 1 μm.
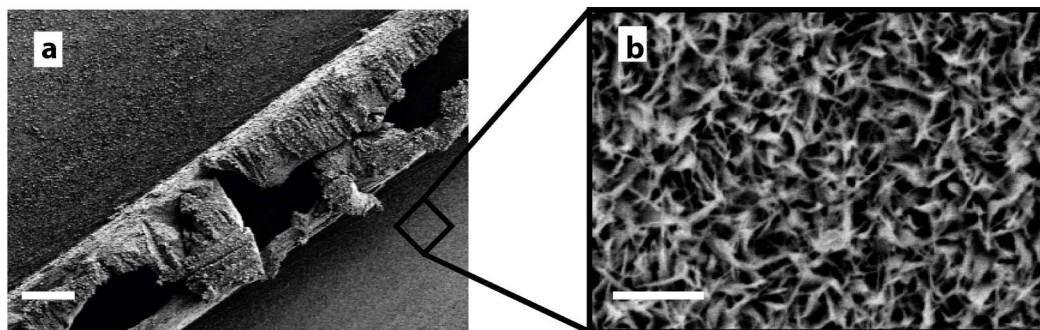
Extended Data Figure 5 | Images of copper oxide substrate surface at different magnifications. **a**, SEM image of the copper oxide nano-textured macro-ridge (height ~100 μm, width ~200 μm); scale bar, 100 μm. **b**, A magnified image, showing spiky nano-textures; scale bar, 1 μm.
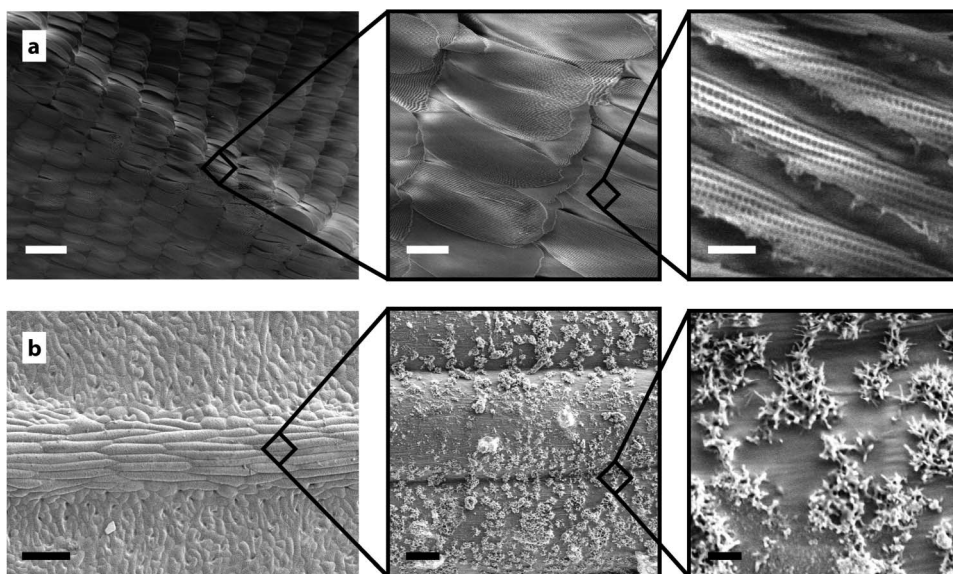
Extended Data Figure 6 | SEM images of naturally occurring surfaces at different magnifications. a, A vein on the wing of a Morpho butterfly (*M. didius*); **b**, a vein on a nasturtium leaf (*T. majus L.*). Scale bars in **a** left to right; 200 μm, 50 μm and 1 μm: scale bars in **b** left to right; 200 μm, 10 μm and 2 μm.
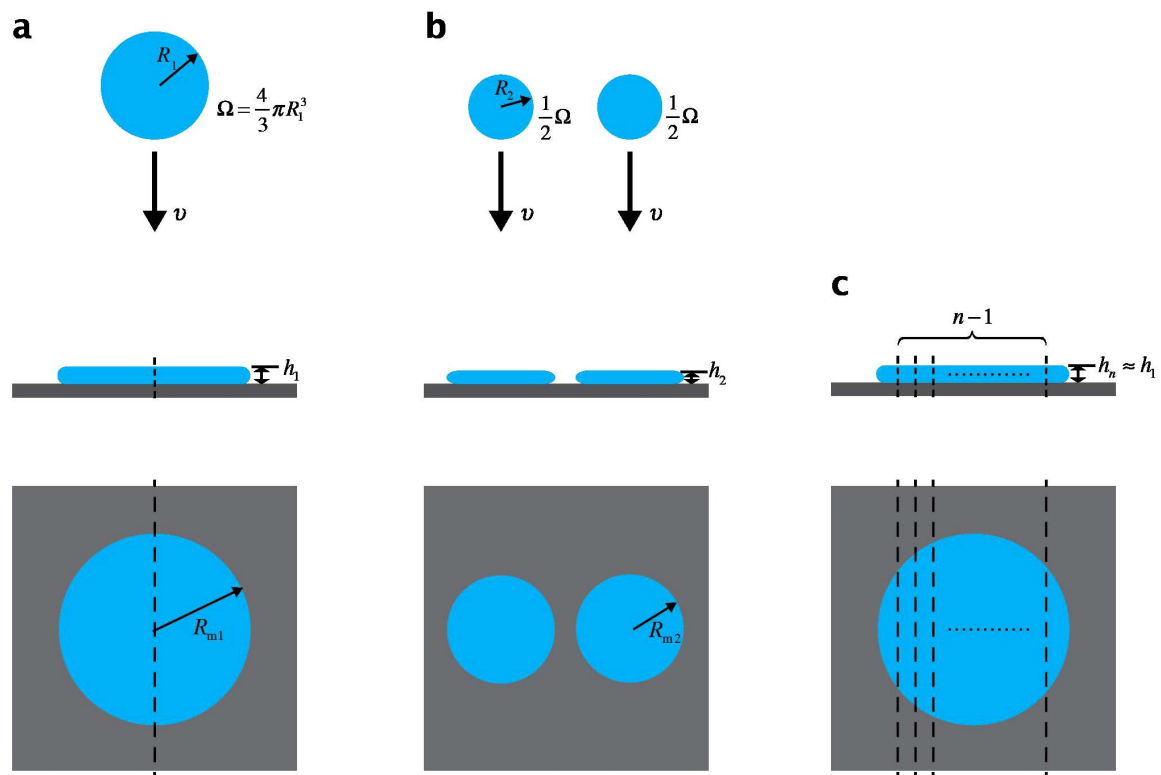
Extended Data Figure 7 | Droplet splitting and contact time. **a–c**, Diagrams of the ridge case (**a**), the simplistic case where a droplet splits before impact (**b**), and the generalized (*n*-split parts) ridge case (**c**).

Extended Data Table 1 | Experimental contact time of bouncing drops from past studies

Study	Droplet	Radius (mm)	Contact time (ms)	**Contact time (dimensionless)**	Ref.
Wachters & Westerling (1966)	water on hot solid	1.15	11.1	**2.4**	28
Richard & Quéré (2000)	water	0.4	2.6	**3**	15
Aziz & Chandra (2000)	molten tin	1.35	13	**2.3**	32
Richard et al. (2002)	water	0.1-5	0.3-50	**2.6**	1
Clanet et al. (2004)	water	1.25	13.5	**2.6**	12
Bartolo et al. (2005)	water	1	16	**4**	20
Legendre et al (2005)	toluene in water	1.3	28	**3.0**	33
Bartolo et al. (2006)	water	1	15	**4**	16
Reyssat et al. (2007)	water	1.2	13 ± 2	**3**	34
Jung & Bhushan (2008)	water	1	16	**4**	35
Brunet *et al* (2008)	water	1.35	23	**4.0**	36
Tuteja et al (2008)	hexadecane	0.72	350	**110**	37
Tsai et al. (2009)	water	1	12.5	**3**	38
Reyssat et al. (2010)	water	1.15	13	**2.8**	21
Mishchenko et al. (2010)	water	1.5	20	**2.9**	8
Li et al. (2010)	water	1.35	14.9-22.3	**2.5-3.8**	22
Zou et al. (2011)	water on water	0.86-2.33	15-62	**4.8[§]**	39
Kwon & Lee (2012)	water	0.022	0.032	**2.6**	40
This paper	water	1.3	7.8	1.4	
	§ Liquid impact on liquid. All other studies liquid drop impacts solid				

CORRECTIONS & AMENDMENTS

Erratum: Reducing the contact time of a bouncing drop

James C. Bird, Rajeev Dhiman, Hyuk-Min Kwon
& Kripa K. Varanasi

In this Letter, the 'received' date should have been 29 June 2012, rather than 29 June 2013. This has been corrected online in the HTML and PDF versions of the paper.